Shock Waves (2007) 17:29–42
DOI 10.1007/s00193-007-0087-9

ORIGINAL ARTICLE

Controlling the form of strong converging shocks by means of disturbances

V. Eliasson · N. Apazidis · N. Tillmark

Received: 19 May 2006 / Accepted: 18 October 2006 / Published online: 20 June 2007

Abstract The influence of artificial disturbances on the behavior of strong converging cylindrical shocks is investigated experimentally and numerically. Ring-shaped shocks, generated in an annular cross sectional shock tube are transformed to converging cylindrical shocks in a thin cylindrical test section, mounted at the rear end of the shock tube. The converging cylindrical shocks are perturbed by small cylinders placed at different locations and in various patterns in the test section. Their influence on the shock convergence and reflection process is investigated. It is found that disturbances arranged in a symmetrical pattern will produce a symmetrical deformation of the converging shockfront. For example, a square formation produces a square-like shock and an octagon formation a shock with an octagonal front. This introduces an alternative way of tailoring the form of a converging shock, instead of using a specific form of a reflector boundary. The influence of disturbances arranged in non-symmetric patterns on the shape of the shockfront is also investigated.

Keywords Shock focusing · Annular shock tube · Imploding shock

PACS 47.10.ab · 47.40.Nm

1 Introduction

Focusing of shock waves can be used to generate high temperatures and pressures. This, together with many technological applications is one of the main reasons for continuing research in this area. A challenging problem is to generate imploding cylindrical shock waves preserving their original shape. It is known, however, that a converging cylindrical shock wave is very sensitive to perturbations and will change its form when encountering a disturbance. It is, therefore, important to clarify the influence of disturbances on the process of shock convergence and reflection. The influence of obstacles on the flow is closely related to two interesting problems. The first one being the relation between the shape and the local strength and thus speed of the shockfront propagation. This means that a highly curved part of the shock wave propagates faster than the adjacent planar part, which leads to a transformation and reorientation of the shock shape. The second problem concerns with the stability of the converging shock.

Shock diffraction is a classic example of shock wave propagation over obstacles. Bryson and Gross [4] investigated plane strong shock diffractions over cones, a cylinder and a sphere. Detailed schlieren photographs of the diffraction show the regular reflection, Mach reflections generating vortexes, triple points and their interaction. Their results were shown to be in good agreement with Whitham's theory [12–14].

A study of shock wave focusing, by Takayama et al. [10], was conducted in a horizontal coaxial annular shock tube. They introduced disturbances in the flow by thin cylindrical rods with three different diameters. Experiments showed that the disturbance behind the shockfront was more significant for rods with larger diameter. The inner body of the shock tube was suspended by four pieces of relatively large diameter cylindrical rods and hence a mode-4 instability was observed, even when larger diameter disturbances were introduced in the flow.

In 1987, Takayama et al. [9] used two different annular horizontal shock tubes, both of which were equipped with n

Communicated by K. Takayama.

V. Eliasson · N. Apazidis (✉) · N. Tillmark
KTH Mechanics, Royal Institute of Technology,
10044 Stockholm, Sweden
e-mail: nap@mech.kth.se

supports for the inner body, and observed an n-mode instability. To test the influence of an initial disturbance on the shock convergence, 12 cylindrical rods were placed in the test section of the shock tube having four supports. At first, the shock wave was deformed by the 12 rods, but when it approached the center of convergence the mode-4 pattern appeared again. It was concluded that it was not possible to completely suppress the disturbances caused by the presence of supports.

Watanabe et al. [11] studied converging cylindrical shocks in a vertical annular shock tube having a self-sustained structure, lacking supports. They were able to produce converging shock waves more uniformly than in a similar horizontal coaxial shock tube with supports. Even in the absence of supports, small disturbances were observed in the flow, presumably caused by small area variations in the coaxial channel. Watanabe et al. [3] distributed cylindrical rods at a certain distance upstream of the test section. Using both 2, 12 and combinations of 4 and 6 rods, they observed that disturbances created by a smaller mode number were stronger than those with higher mode number.

There is a close connection between the original shock shape and its preservation of symmetry during the focusing process. Schwendeman and Whitham [7] showed analytically that for shocks with regular polygonal shape the original shape was periodically repeated during convergence. Apazidis and Lesser [2] showed this feature numerically in the case of a smooth pentagonal converging shock wave. In an experimental study of a reflection and convergence process in a chamber with a smooth pentagonal reflector, Apazidis et al. [1], confirmed the previous analytical and numerical results in this area. Due to limitations in the experimental setup it was not possible to see the complete cycle of the shock reorientation during the focusing procedure.

The complete shock reorientation cycle was first observed experimentally in Eliasson et al. [5]. In this study, strong shock waves of various forms were produced by changing the shape of the outer boundary of the test section placed at the rear end of the horizontal shock tube. It was verified, for the first time, that octagonal and pentagonal converging shocks successively reorient and repeat the original shape during the focusing process. This is caused by the nonlinear dynamics of the shock propagation and stems from the fact that corners of the shock with high curvature move faster than the adjacent plane sides. The shock wave changes its shape as corners undergo Mach reflection and transform to plane sides. Unlike predictions provided by linear perturbation theories, slightly perturbed shock shapes never grow to catastrophic deformation but will obey the nonlinear deterministic system, which simply means the onset of Mach reflection.

In the present paper, we show a new way of producing converging shock waves of various shapes. Using the same shock tube as in [5] but instead of changing the shape of the outer boundary of the test section, we distribute cylindrical rods inside the test section. The rods are arranged in various positions and patterns and hence can create any disturbance shapes as desired. In the present experiment we study how the shock focusing and reflection is influenced by artificial disturbances. The present numerical work is based on the artificially upstream vector splitting scheme (AUFS) for solving the Euler equations introduced by Sun and Takayama [8]. Good agreement is found between the numerical simulations and the experimental results.

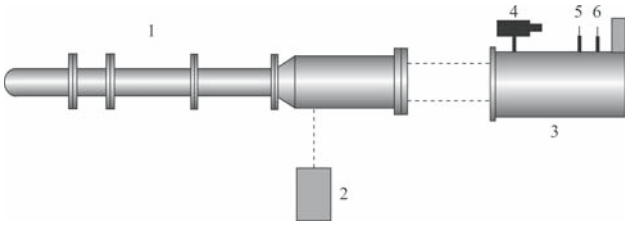

Fig. 1 Schematic overview of the experimental setup: *1* shock tube, *2* pulse laser, *3* schlieren optics, *4* PCO CCD camera, *5* lens and *6* schlieren edge

In Sect. 2 we describe the experimental setup in detail: the shock tube, the visualization technique and artificial disturbances. Section 3 presents experimental results. In Sect. 4 the numerical results are showed and compared with experiments. In Sect. 5, we conclude and summarize the present study.

2 Experimental setup

The experimental setup is shown in Fig. 1 and consists of a horizontal shock tube, schlieren optics and a laser as light source. The shock tube has a test section consisting of a thin cylindrical chamber, in which cylindrical shock waves converge and reflect. The shock wave is visualized using schlieren optics. Schlieren images are recorded by a CCD camera.

2.1 The shock tube

Figure 2 shows the 2.4 m long and 80 mm diameter shock tube, which consists of a high pressure chamber and a low-pressure channel separated by a 0.5 mm thick aluminum diaphragm. To create a shock wave, first the low pressure driven section is evacuated and then the driver section is filled with high pressure gas. The pressure difference across the diaphragm causes it to rupture, driving a shock wave. To achieve a controlled diaphragm opening, we use a cross-arranged knife at the low pressure channel entrance. The knife helps to evenly burst the diaphragm. The shock wave becomes planar while propagating along the low pressure

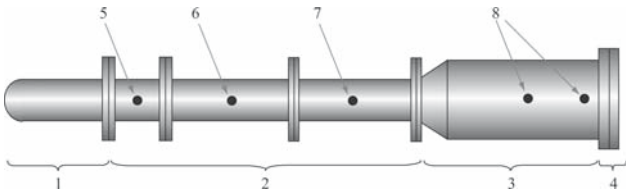

Fig. 2 Schematic overview of the shock tube setup: *1* high pressure part, *2* low pressure part: inlet section, *3* low pressure part: transformation section, *4* low pressure part: test section, *5* low pressure sensor, *6* vacuum valve, *7* vacuum pump, and *8* shock sensors

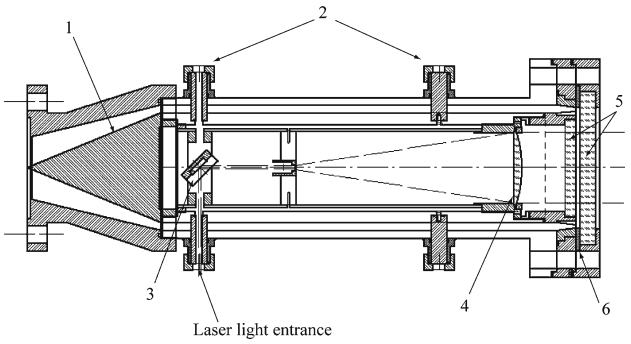

Fig. 3 The annular part of the shock tube:*1* inner body with a cone, *2* supports, *3* mirror, *4* lens, *5* glass windows for visualization, and *6* test section where the obstacles are positioned

channel, then enters the transformation section where it obtains annular cylindrical shape.

The transformation section consists of a conically diverging section, along which the diameter increases from 80 to 160 mm as seen in Fig. 3. The cross-section area is kept constant from the inlet section through the transformation section. An inner body is mounted coaxially in the outer larger diameter tube, which forms the annular section. The 490 mm long and 140 mm diameter inner body is suspended by two sets of four supports. The supports are shaped as wing profiles in order to minimize the disturbances in the flow. The second set of supports is angularly displaced by 45° relative to the first set. The plane test section is mounted directly at the end of the annular section. Hence, the shock wave can enter into the test section via a sharp 90° bend eventually to focus and reflect. The gap width of the cylindrical parallel test section between the two facing glass windows is 5 mm and, therefore, the cross section area is one half of that of the annular part. The outer boundary of the test section is circular. The test gas in the present experiments is air at 13.3 kPa at room temperature and the driver gas is also air at about 1,500 kPa at room temperature. This pressure ratio produces strong shock waves at Mach number 2.3.

The shock speed, U_s, is measured by thin-film heat transfer gauges placed along the annular section, with which the temperature jump across the shock waves is detected and the shock speed estimated within the accuracy of 0.5%.

2.2 The shock visualization

An Nd:Yag laser (NewWave Orion) emitting a 5 ns light pulse is used as light source for the schlieren optics. As shown in Fig. 3, the light beam is introduced into the shock tube perpendicularly to the tube axis and then deflected in the axial direction by a mirror placed inside the inner tube. To minimize spurious reflections from the inner side of the inner tube the walls are coated with non-reflective material. To form a parallel light beam for the schlieren optics, an adjustable beam expander is mounted inside the inner tube. The parallel light beam passing through the test section is then forming the schlieren images in the receiving optics. A 1.0 mm diameter pin head is placed at the focal plane of the image lens as schlieren knife-edge. It intercepts parts of the light beam to exhibit schlieren effects before reaching an image plane of a CCD camera (SensiCam, 12 bits, 1,280 × 1,024 pixels, pixel size 6.7 × 6.7 μm, CCD). The CCD camera and the light source laser are triggered by an output signal from the shock sensors via a properly adjusted time-delay unit. The delay unit (Stanford Research System, DG535) retards the output signal with a properly preset value to synchronize schlieren images at expected positions in the test section.

2.3 Artificial disturbances

Artificial disturbances are introduced in the flow by 1–16 cylinders with three different diameters (7.5, 10 and 15 mm). The cylinders are placed at two radial positions, $r_1 = 46.25$ mm and $r_2 = 66.25$ mm, in both regular and irregular patterns using a template with holes as shown in Fig. 4 a. Figure. 4b shows an example of 16 cylinders of 10 and 15 mm diameters placed at $r = r_1$.

3 Experimental results

Gas temperature is an important parameter in determining the speed of sound and thus the Mach number. We therefore checked, using a cold wire, the temperature variation during the pressure adjustment in the low pressure section of the shock tube. We found that the temperature reached a constant value 1 min after final adjustment of the pressure. Figure 5 shows the temperature variation during the pressure adjustment. Before time instant (I), the gas is at low pressure and in thermal equilibrium with its confinement. Between (I) and (II) the gas is supplied to the driven section and the temperature rises. Between (II) and (III) the gas is cooled by the surrounding walls. The vacuum pump is started at (III) to decrease the pressure to 13.33 kPa and stopped at (IV). The temperature first falls due to the gas expansion and then rises to ambient value within approximately 1 min.

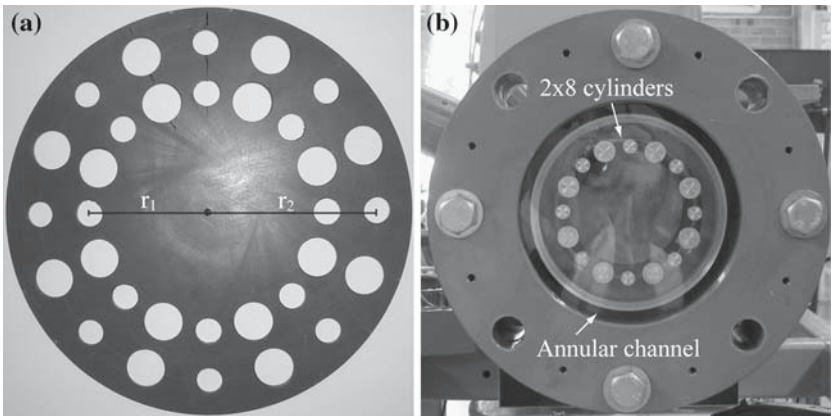

Fig. 4 **a** Template for cylinder positioning, $r_1 = 46.25$ mm and $r_2 = 66.25$ mm. **b** Rear part of the shock tube with 2×8 cylinders placed in the test section at $r = r_1$

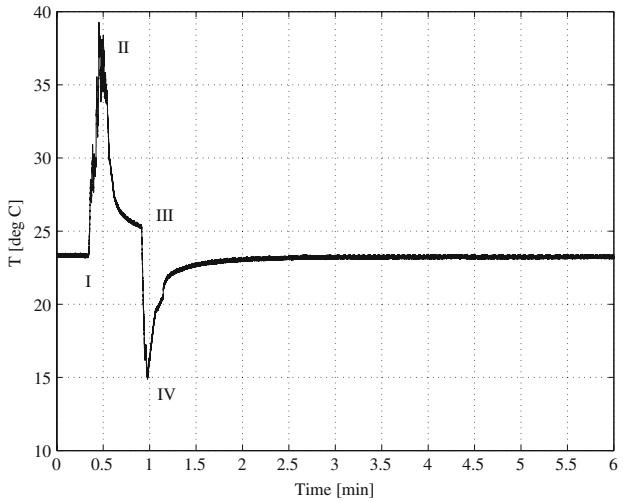

Fig. 5 The temperature in the low pressure part during evacuation

An initially cylindrical shock wave is disturbed by interacting with cylindrical obstacles placed in the test section. The shock wave diffracted over the cylindrical obstacles eventually produces series of Mach reflections which move toward the center of convergence. Present results show that a symmetric pattern of obstacles eventually produces a regular shock wave with plane sides and corners which will repeat its shape in successive intervals. It is thus possible to create shock waves of various polygonal shapes, for example octagons, by introducing corresponding polygonally distributed obstacles. The present study agrees with earlier analytical, numerical and experimental results obtained by Schwendeman and Whitham [7], Apazidis and Lesser [1] and Eliasson et al. [5], which also show that polygonal shock shapes are successively repeated. Unlike our previous experiment, in this case the polygonal shock shape is obtained not by the reflection from the polygonal reflector, but by the interaction with distributed cylindrical obstacles placed in the test section. Their influence on the shock form depends on the diameter of obstacles. Cylinders with larger diameters generate more significant disturbances. This agrees with the results of Takayama et al. [9].

First, a single 15 mm diameter cylinder was placed at $r_1 = 46.25$ mm in the test section. In Fig. 6, a schlieren photograph shows the converging shock shape after passing over the cylinder. A reflected shock wave (RC) is created upon the converging shock's impingement on the cylinder. After diffraction over the rear side of the cylinder, a three-shock system consisting of a Mach shock (MS), a converging or incident shock (CS), and a reflected shock (RS) forms a

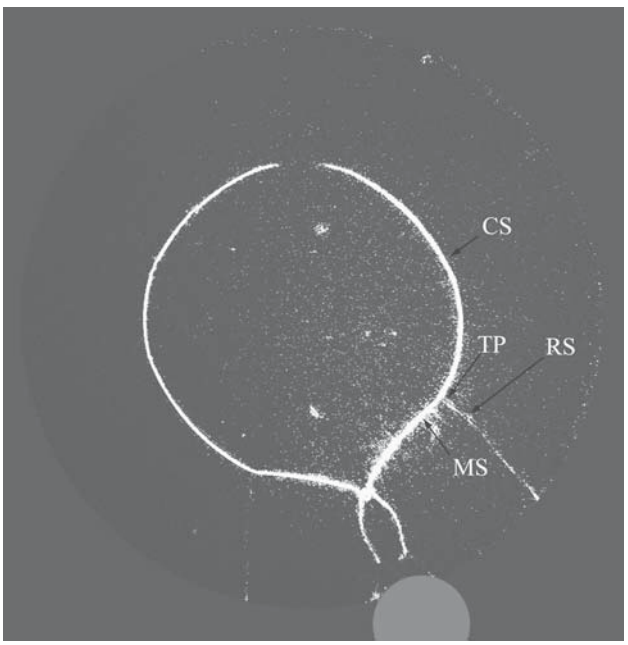

Fig. 6 Schlieren photograph of a shock wave passing a single 15 mm diameter cylinder. $M_S = 3.2$. CS converging cylindrical shock, RS reflected shock from the cylinder, MS Mach shock and TP triple point. The *grey filled circle* shows the position of the cylindrical obstacle

triple point (TP) as seen in Fig. 6. Photographs taken at different time instants are displayed in superposition in Fig. 7. We can readily compare the evolution of shock shapes and wave interactions. Comparing our results with Bryson and Gross [4], we can see similar behavior in planar shock diffraction over a cylinder. The difference is in the shape of the incoming, reflected and converging shocks.

Second, two 15 mm diameter cylindrical obstacles were placed at $r_1 = 46.25$ mm opposite each other. Sequential images are shown in Fig. 8 which is similar to Fig. 7. Here it is clearly observed that parts of the shock wave are delayed when passing over an obstacle.

To compare the effect of the diameter size on the shock shape, we replaced one of the two cylinders by a smaller one with a diameter of 7.5 mm. Four sequential images are presented in Fig. 9. It is now possible to see the influence of the diameter on the shock shape and propagation. We can see a clear asymmetry in the shock shape due to the difference in the diameters. On the rear side of the smaller cylinder, a second Mach shock and a triple point are visible. This was also observed in schlieren photographs of planar shock diffraction over a cylinder [4] when the incident shock wave passed about 0.5– 1.0 diameter past the rear stagnation point of the cylinder. The secondary Mach shock appears due to collision of the two initial Mach shocks.

Third, we performed a series of experiments with three 15 mm diameter cylinders placed at $r_1 = 46.25$ mm in a right isosceles triangle formation. The result of sequential visualization of converging shocks is shown in Fig. 10 in a similar way as in the previous displays. Plane Mach shocks develop after the shock diffraction over the cylindrical obstacles. The original circular shock shape tends to build plane sides with

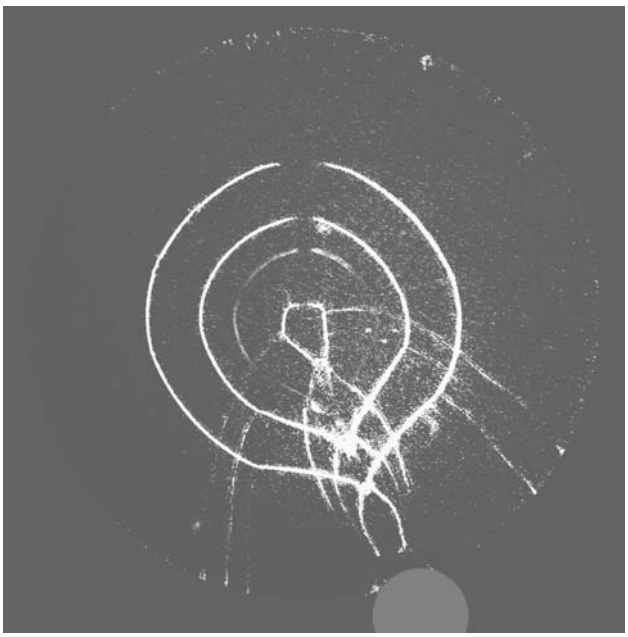

Fig. 7 Schlieren photograph of four shock waves at different time instants passing a single 15 mm diameter cylinder. $M_S = 3.2$. The *grey filled circle* shows the position of the cylindrical obstacle

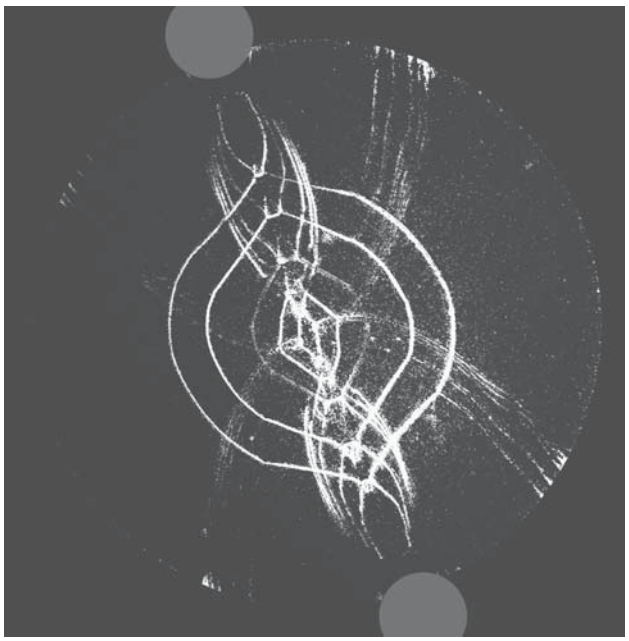

Fig. 8 Schlieren photograph of converging shock waves at five different instants. Two 15 mm diameter cylindrical obstacles are placed opposite each other. The *grey filled circles* show the positions of the cylindrical obstacles

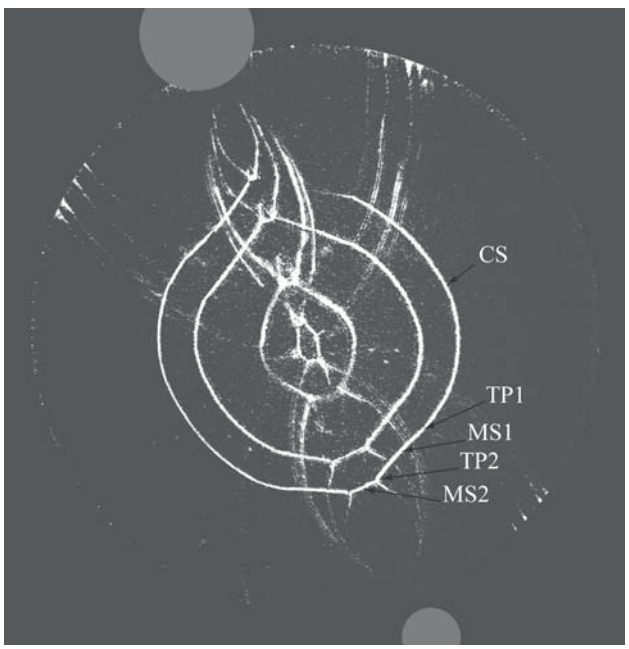

Fig. 9 Schlieren photograph of four shock waves at different time instants passing a 15 and 7.5 mm diameter cylinders. $M_S = 3.2$. CS converging cylindrical shock, RS reflected shock from the cylinder, MS, Mach shock and TP, triple point. The *grey filled circles* show the positions of the cylindrical obstacles

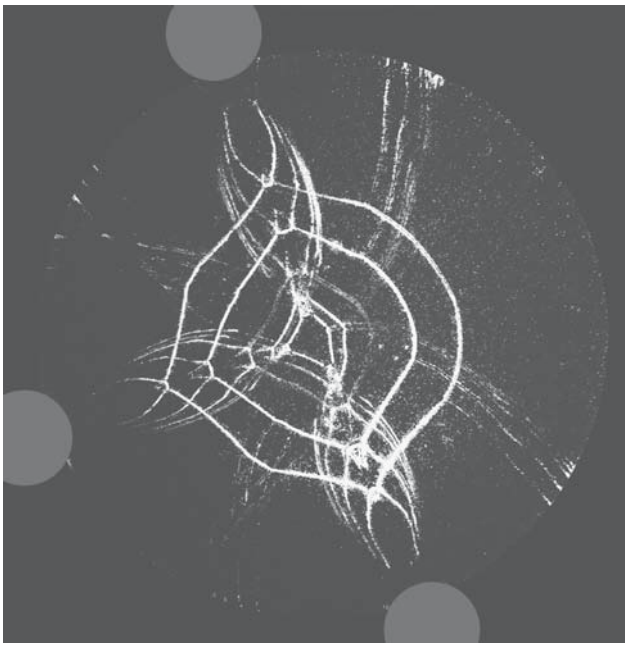

Fig. 10 Schlieren photographs of five shock waves at different time instants passing three 15 mm diameter cylinders. The grey filled circles show the positions of the cylindrical obstacles

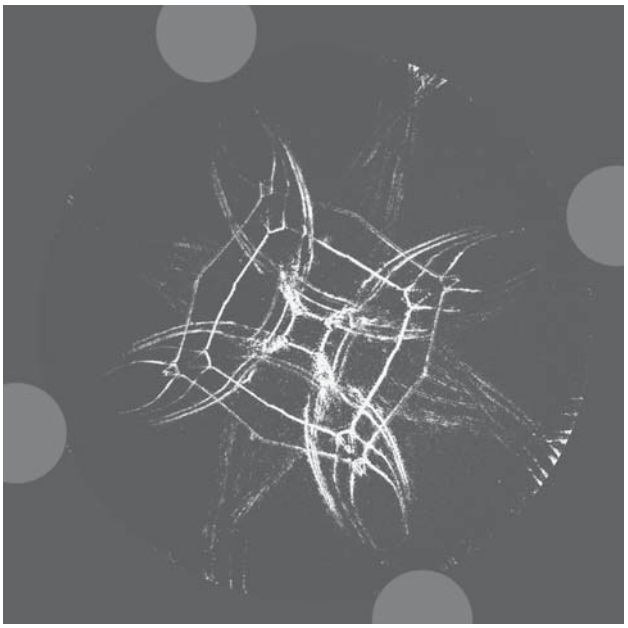

Fig. 11 Schlieren photographs of a shock wave at five different time instants passing four 15 mm diameter cylinders. The *grey filled circles* represent the cylindrical obstacles

sharp corners even in the undisturbed part of the shock as the shock approaches the center. The undisturbed part also travels faster than the disturbed part of the shock.

To create a square-like shock shape, we placed four 15 mm diameter cylinders at $r_1 = 46.25$ mm in a square formation. Corresponding sequential schlieren images are shown in Fig. 11. At first, eight sides, which are convex, form an octagon with square-like shape. As the shock wave approaches the center the sides become plane and the octagon is replaced by a square.

Figure 12 shows the deviation of shock wave radii normalized by the mean radius at $\Delta t = 200$ μs, $\Delta t = 205$ μs, $\Delta t = 210$ μs and $\Delta t = 215$ μs in the case of four cylindrical obstacles. The time delay, Δt, is defined to be the time interval between the instant when the shock passes the second sensor and that when the photograph is taken. In the first frame, $\Delta t = 200$ μs, a slightly perturbed octagonal shape is observable. At later time, the Mach shock parts forming the sides, become more planar.

Next we placed eight 15 mm diameter cylinders at $r_1 = 46.25$ mm in an octagonal formation. After interaction with the obstacles, the shock shape becomes that of an octagon with curved concave sides as seen in Fig. 13a and b and then transforms into a polygon with 16 sides as shown in Fig. 13c. At a later instant, the shock wave transforms to an octagonal shape again as seen in Fig. 13d. The second octagonal shock shape is rotated by 45° with respect to the initial shape. This is an experimental confirmation of the polygonal shock

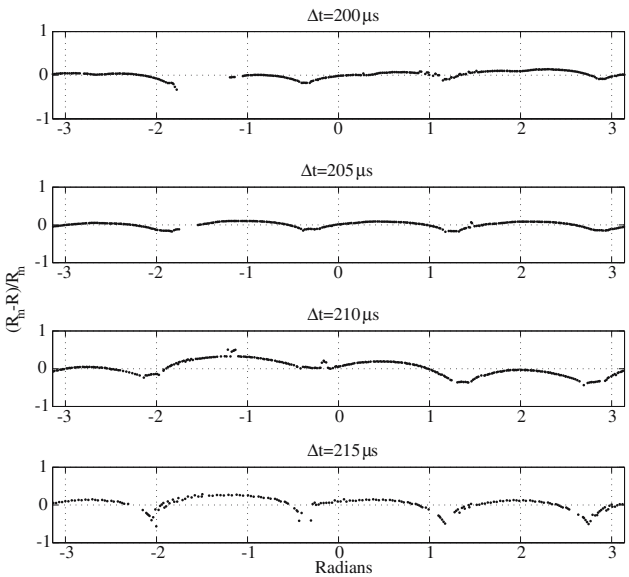

Fig. 12 The deviation from the mean radius normalized with the mean radius for the case with four cylinders placed at the corners of a square. The time delay, Δt, for the individual shock waves are 200, 205, 210 and 215 μs, respectively

dynamics predicted earlier analytically [7], and numerically [2]. Eliasson et al. [5] confirmed experimentally this trend by using a different approach for shock formation.

The reflected shock wave displayed in Fig. 13f and g shows that a circular shape is obtained at the early stage of shock reflection. Eliasson et al. [5] found that the shock was later

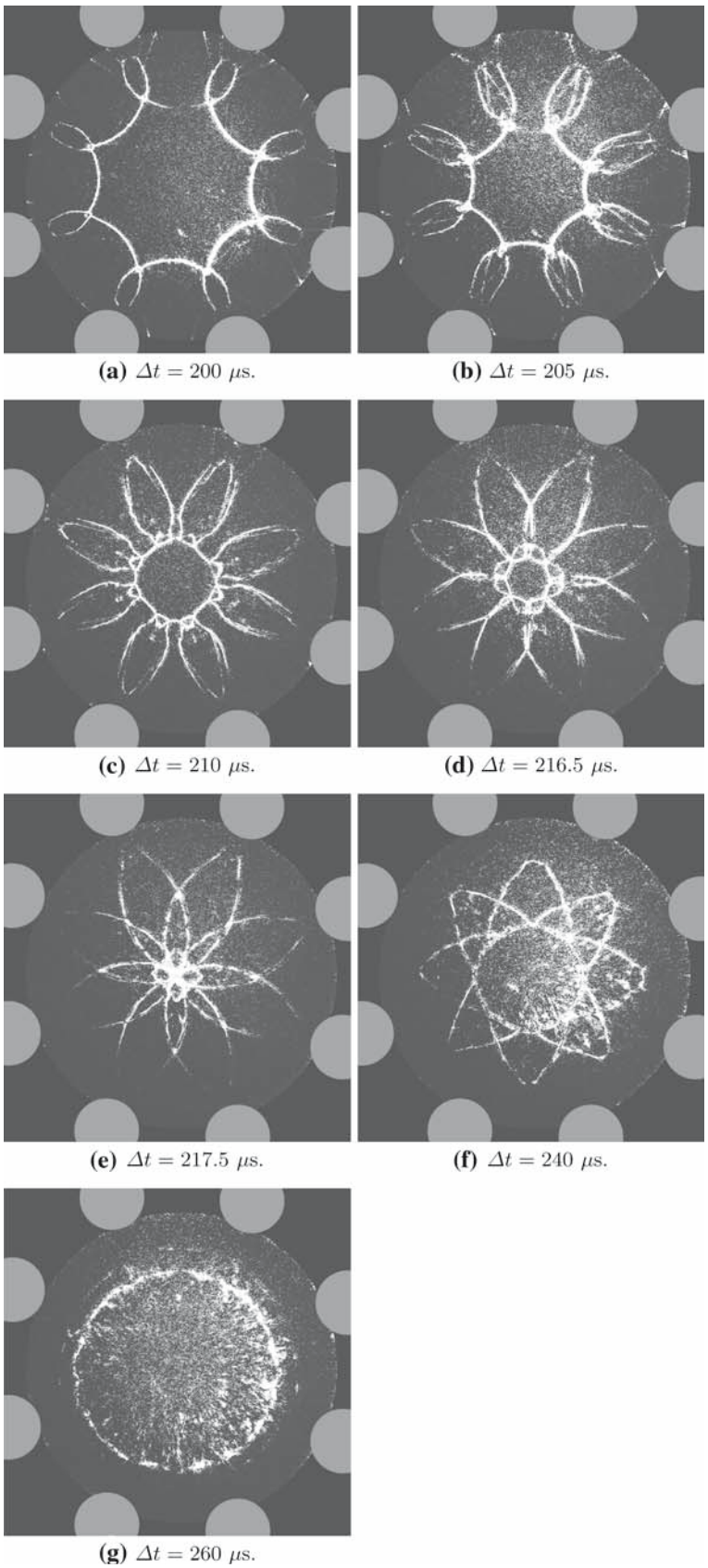

(a) $\Delta t = 200\ \mu$s. **(b)** $\Delta t = 205\ \mu$s.

(c) $\Delta t = 210\ \mu$s. **(d)** $\Delta t = 216.5\ \mu$s.

(e) $\Delta t = 217.5\ \mu$s. **(f)** $\Delta t = 240\ \mu$s.

(g) $\Delta t = 260\ \mu$s.

Fig. 13 Schlieren photographs of shock waves at different time instants passing eight 15 mm diameter cylinders. The *grey circles* represent the cylindrical obstacles

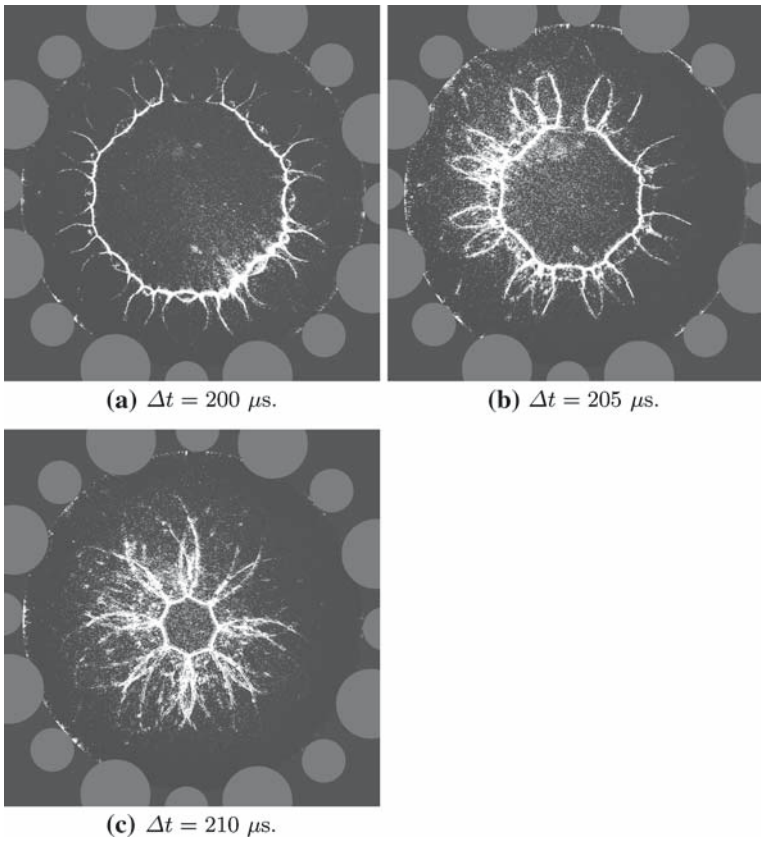

Fig. 14 Schlieren photographs of shock waves at three different time instants passing sixteen 15 and 10 mm diameter cylinders. The *grey filled circles* show the positions of the cylindrical obstacles

affected by waves and flow behind the converging shock, which eventually resulted in an octagonal shape.

To further investigate the effect of the size of cylindrical objects, we studied shock interaction with more complex obstacle formations. The first formation we looked at was a combination of eight 15 mm diameter cylinders and eight 10 mm diameter cylinders distributed in two symmetric octagonal formations as shown in Fig. 14. Initially the influence of all 16 cylinders is present. The shock shape appears to contain 16 concave fronts but has still an octagon form. Disturbances generated by the interaction with larger diameter cylinders overtake those created by the smaller ones as the shock wave is approaching the center of convergence, and again a shock with an octagonal shape is formed.

To examine the effect of asymmetrical blockage, we placed several cylindrical objects in a dense formation at a certain angular position leaving the rest of the chamber free. Three 15 mm diameter and two 10 mm diameter cylinders where placed at $r_1 = 46.25$ mm while three 7.5 mm diameter cylinders at $r_2 = 66.25$ mm, at the same angular position as 15 mm diameter cylinders, as shown in Fig. 15. At such high blockage ratio, the disturbed part of the shock was attenuated and delayed.

From the schlieren images in Fig. 16, we observed that the center of individual shockfronts shifted as a result of the asymmetrical blockage. The schlieren images of the shockfronts are used to calculate the radial distance and the center point. The calculated curves are then centered at a common origin and displayed together with the schlieren images in Fig. 16. If the center of the individual shock waves did not shift, the calculated and the visualized shockfronts would overlap exactly. The calculated fronts of the largest two shock waves at 200 and 210 μs overlap with the schlieren images. However, the calculated front of the third shock wave at 215 μs does not overlap. Hence, we can conclude that the center of the shockfront is shifted toward the obstacles. This agrees with previous observations made by Perry and Kantrowitz [6]. However, the influence of the disturbances on the shock shape is more significant than that on the deviation of its center. Thus the deviation of the convergence center is small as compared to the shockfront deformation.

4 Numerical results

In our previous work [5], we used the artificially upstream flux vector splitting scheme (AUFS) for solving the two-dimensional Euler equations, introduced by Sun and Takayama [8]. In the present work this scheme once again was able to accurately predict and reproduce the major features of the shock propagation process.

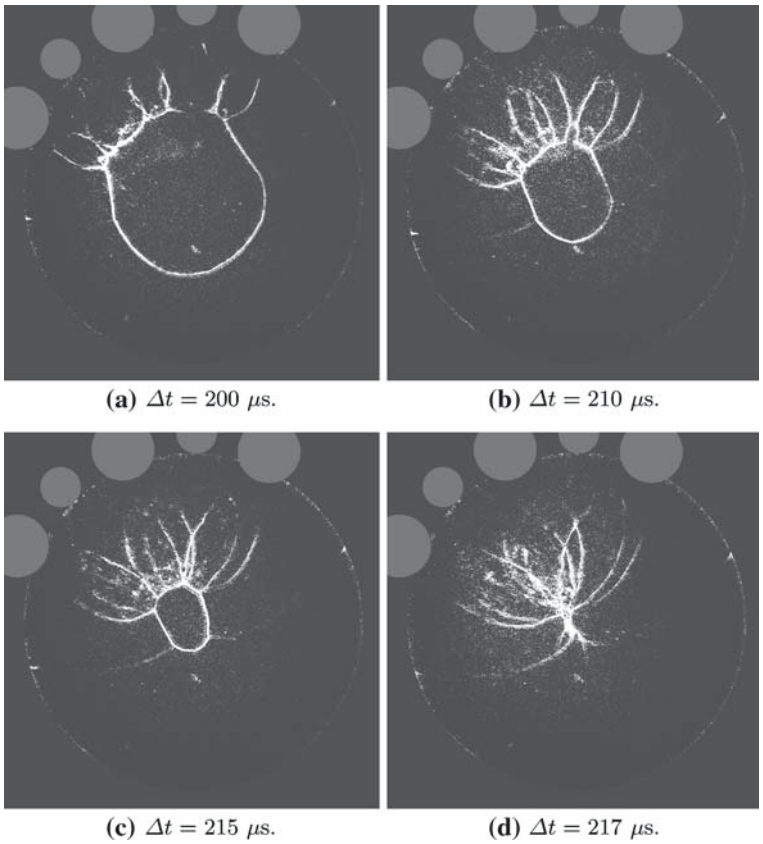

Fig. 15 The shock wave at different instants, $M_s = 2.3$. The *grey filled circles* show the positions of the cylindrical obstacles. Three additional 7.5 mm diameter cylinders are not seen in the figure, placed outside the 15 mm diameter cylinders

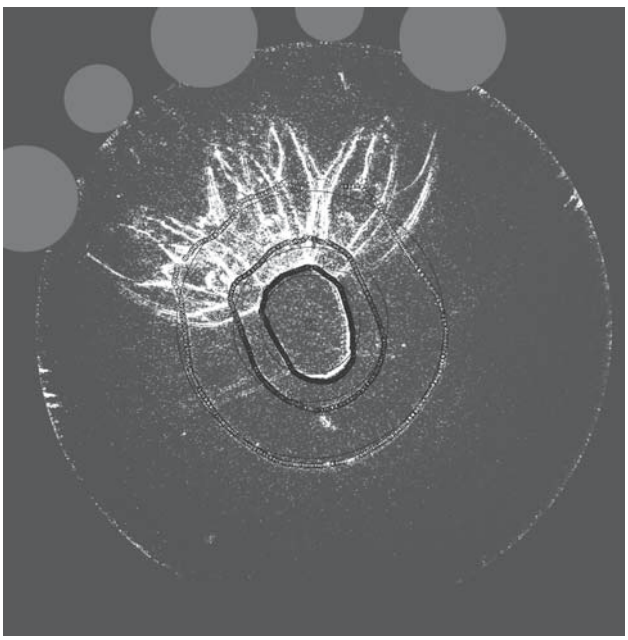

Fig. 16 Schlieren photographs of three converging shock waves, (same as the first three photographs in Fig. 15), a calculated front of the shock wave and a calculated center point

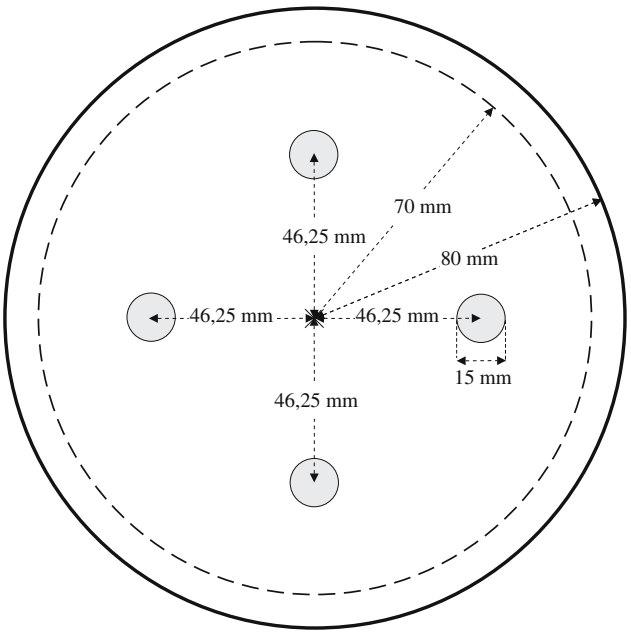

Fig. 17 The outer cylindrical computational domain boundary with the thin adjacent initial high pressure zone and four cylindrical obstacles

We consider the propagation of a strong shock in the computational domain representing the shock tube test section. As explained earlier, the test section is a thin cylindrical chamber mounted at the rear end of the shock tube. Shocks are created upon the release of a high pressure in a thin annular outer boundary and propagate into the inner part of the test

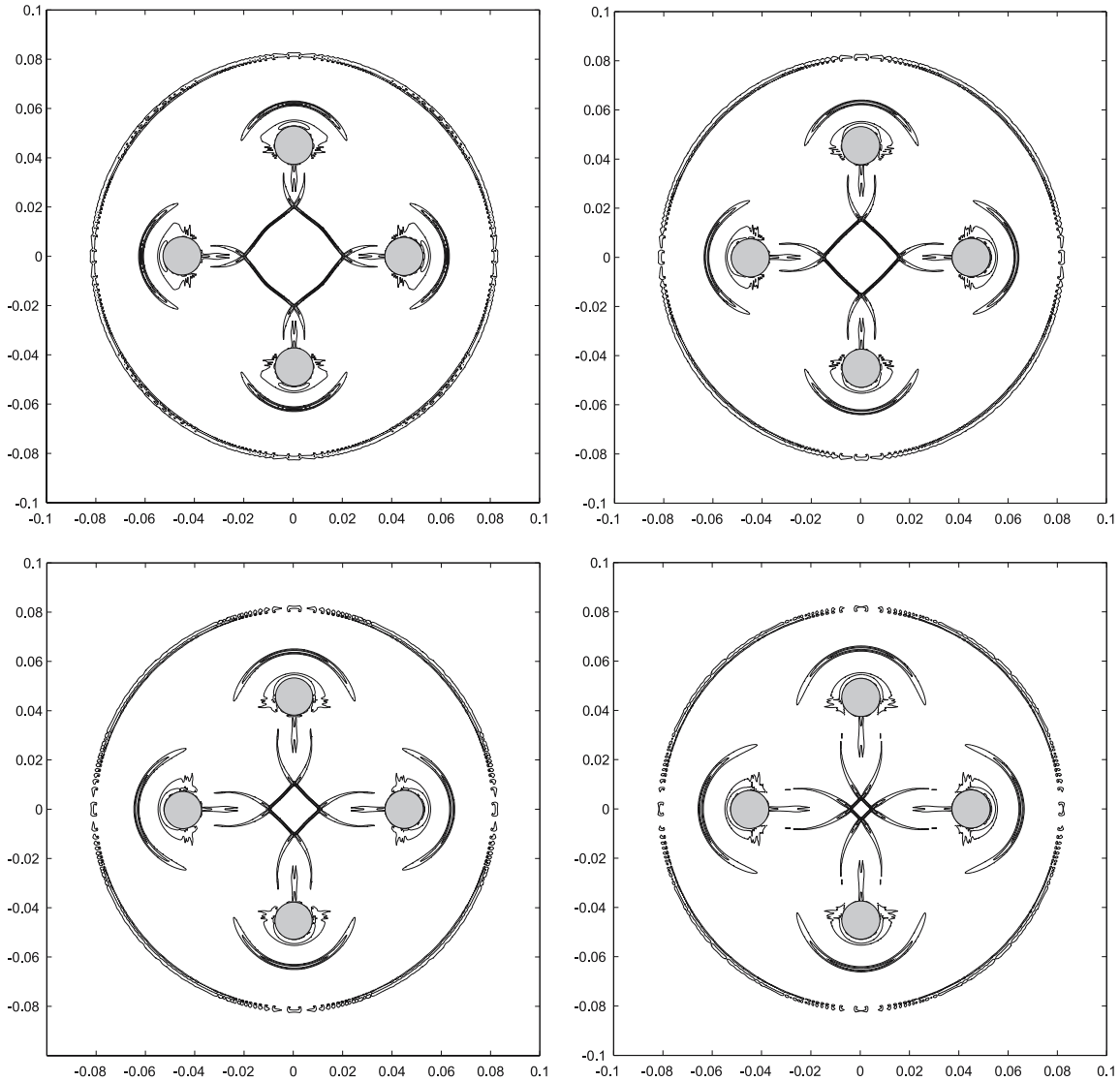

Fig. 18 Density gradient profiles at various positions for the case of four cylindrical disturbances

section, initially kept at lower pressure. Cylindrical obstacles of various radii are placed in various formation patterns in this domain.

The pressure in the inner of the test section is set to 13.3 kPa, in all considered cases, the same value as in the experiment.

The pressure loss for a shock propagating along the straight shock tube is small; however, it may be significant at the sharp 90° bend. Eliasson et al. [5] numerically simulated shock attenuation and losses at the sharp 90° bend and indicated a significant decrease in Mach number after the bend. One of the measured and calculated parameters of the complete flow was the average radius of the converging and reflected shock in the computational domain as a function of time. These curves were calculated for various initial pressure ratios starting from the maximum theoretical ratio of 112 and gradually decreasing this value in order to account for the pressure losses in the tube. The pressure ratio value that compared best with the experimental curves was found to be about 30% of the maximum value, giving $p_4/p_1 = 33.6$. This value was used in the present calculations as well.

The convergence of the initial cylindrical shock, its interaction with cylindrical obstacles placed in various formation patterns, and the following reflection process from the center are studied in detail and results are compared with the experimental observations. The computational domain including a thin high-pressure zone adjacent to the domain boundary and a typical configuration of cylindrical obstacles are schematically shown in Fig. 17.

The density gradient profile at various positions is shown in Fig. 18 for the four cylindrical obstacles in a square

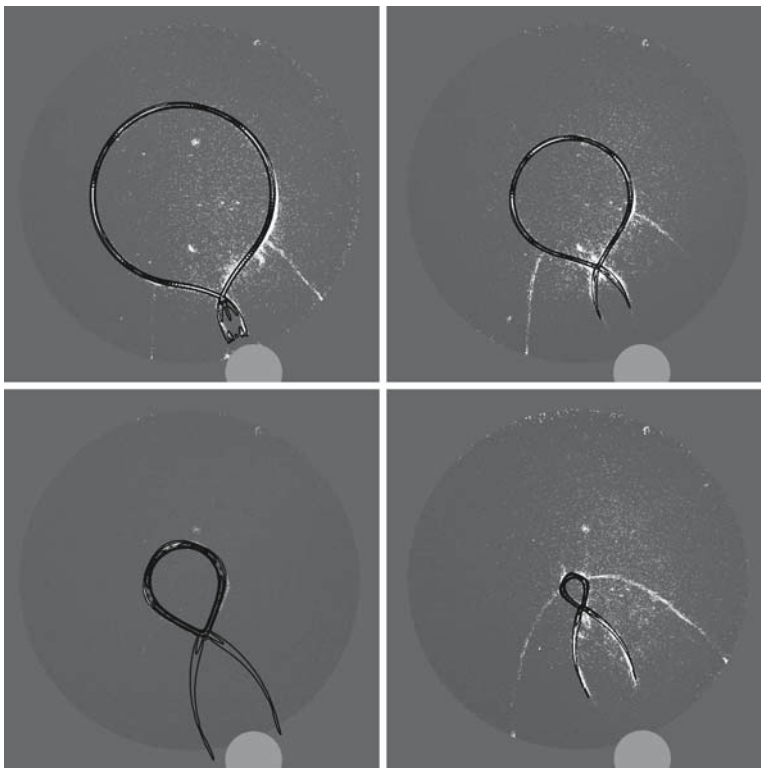

Fig. 19 Comparison of the calculated shockwave profiles with the experimental schlieren images with one cylindrical disturbance for $p_4/p_1 = 33.6$

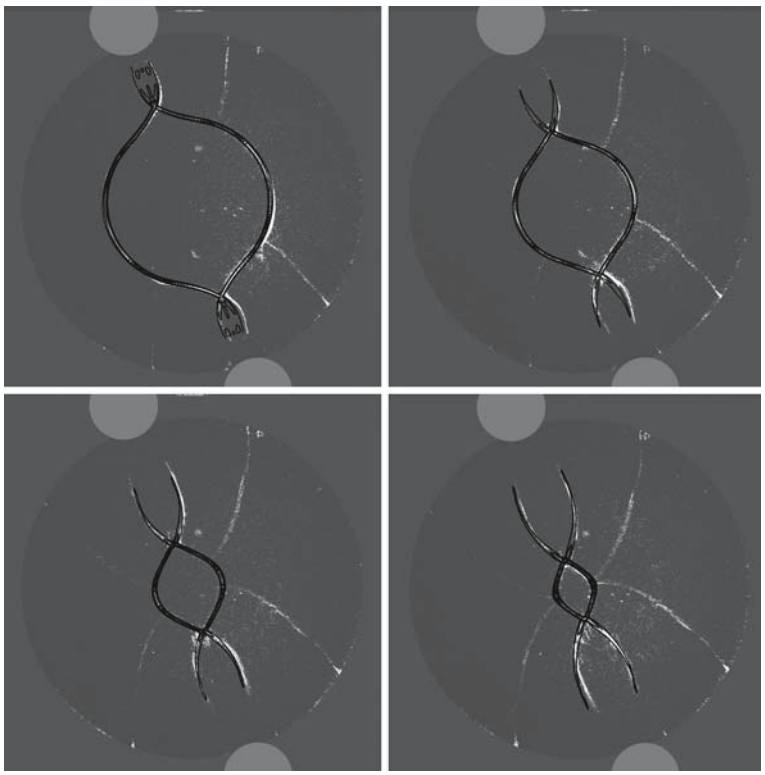

Fig. 20 Comparison of the calculated shockwave profiles with the experimental schlieren images at various positions with two cylindrical disturbances for $p_4/p_1 = 33.6$

formation. In the beginning, the diffracted shock wave appears to be convex similar to experimental observations. A square-like shock shape is formed at a later stage as the shock propagates toward the center. Similar to experimental observations, the sides of the shockfront become plane as shown in Fig. 11.

A comparison of the numerical and experimental results for one, two, four and eight cylindrical obstacle cases are

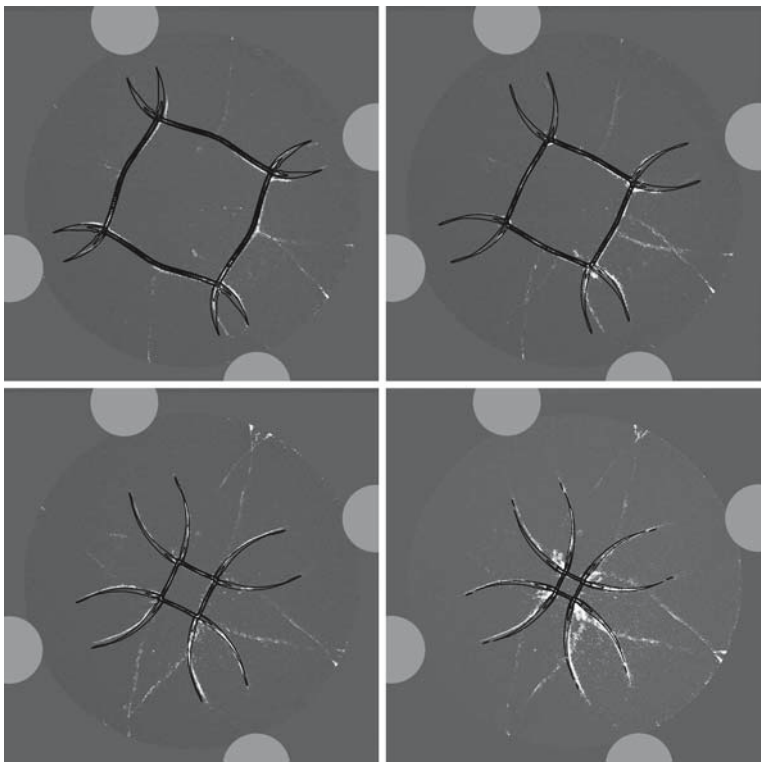

Fig. 21 Comparison of the calculated shockwave profiles with the experimental schlieren images at various positions with four cylindrical disturbances for $p_4/p_1 = 33.6$

shown in Figs. 19, 20, 21 and 22. As we can see the AUSF scheme reproduces the main features of the shock propagation. The simulated converging shock shapes agree well with experimental ones. The numerical shockfronts are displayed as black curves overlapping the white experimental shock shapes.

Figures 21 and 22 show that it is possible to obtain converging shocks with polygonal form by means of cylindrical obstacles placed in the computational domain. In Fig. 21 four cylindrical obstacles are placed symmetrically resulting in a square shock shape, while in Fig. 22 an octagonal shock shape is produced with eight cylindrical obstacles. Alternatively, various converging shock shapes may be produced by adopting an appropriate form of the reflector boundary as reported earlier in [5]. The present method is simpler in terms of practical applications. However, losses due to disturbances in the flow is one of the topics for further discussion. In other words, one would like to compare numerically the development of the maximum shock Mach number during the convergence process in both cases. Figure 23 shows that the maximum Mach number (at a certain time over the whole computational domain) is higher in the case of an octagonal reflector as compared to eight 15 mm diameter cylindrical obstacles. The dashed line represents the maximum shock Mach number for the eight cylindrical obstacles. The first sharp increase in shock Mach number at $t = 20$ μs is due to the area contraction in the flow introduced by the obstacles. The second sharp increase is created at the center of convergence and a gradual decrease of the shock strength follows during the reflection.

5 Conclusions

A horizontal coaxial shock tube was used to study the convergence and reflection of strong shock waves. The interaction of converging shock waves with cylindrical obstacles with three different cylinder diameters was visualized. The cylindrical obstacles were distributed in various patterns. A numerical study was performed and the results were compared with the visualization. The main results are summarized as follows:

(1) We succeeded in generating various polygonal shock shapes by introducing cylindrical obstacles in polygonal formation patterns. The method proposed herein is easier to implement than the one in which the shock is formed by the test section boundary [5]. Since a converging cylindrical shock wave is unstable, it is easy to disturb it and transform the shape of the shock.
(2) The nonlinear, shock-dynamic effect of the evolution of converging polygonally shaped shocks is well demonstrated in the present experiments. An octagonal shockfront transforms into a double octagon and then reconfigures to an octagonal shape although the phase

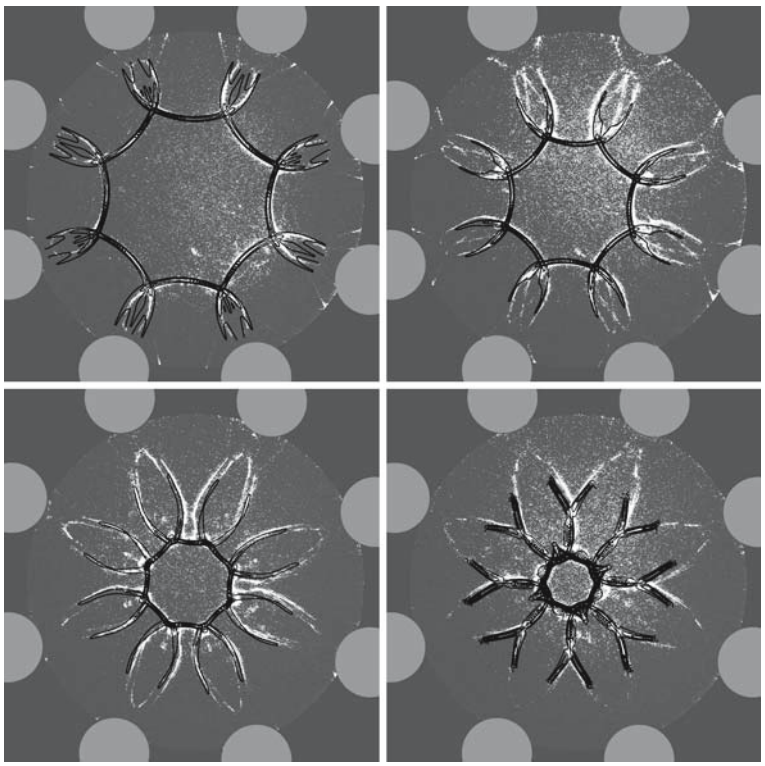

Fig. 22 Comparison of the calculated shockwave profiles with the experimental schlieren images at various positions with eight cylindrical disturbances for $p_4/p_1 = 33.6$

of its orientation is shifted. We thus confirmed experimentally the coupling between the local form of the shock and its local propagation velocity.

(3) Artificial disturbances placed in the test section are more prominent than the disturbances inherited from four supports of the shock tube inner body. The later are suppressed and not observable here as the supports were shaped to minimize initial disturbances.

(4) The diverging reflected shock propagating from the center of convergence is stable and initially of circular shape regardless of the degree of converging shock wave deformation. The form of the shock at farther distances from the center was not visualized here. It is known however that the shock form will be affected by the non-uniform flow created by the converging shock as reported by Eliasson et al. [5].

(5) Diffracted shock waves over cylindrical obstacles are delayed. The center of the converging shock wave is slightly deviated toward the disturbed side. However, the presence of the cylindrical obstacles more significantly affects the shock shape than the shift of the shock center.

(6) Numerical simulations based on the AUFS scheme successfully reproduced the major features of the shock propagation process. The numerical shock motion and flow patterns agreed well with experimental observations. This numerical scheme may therefore serve for a future extension of experimental works.

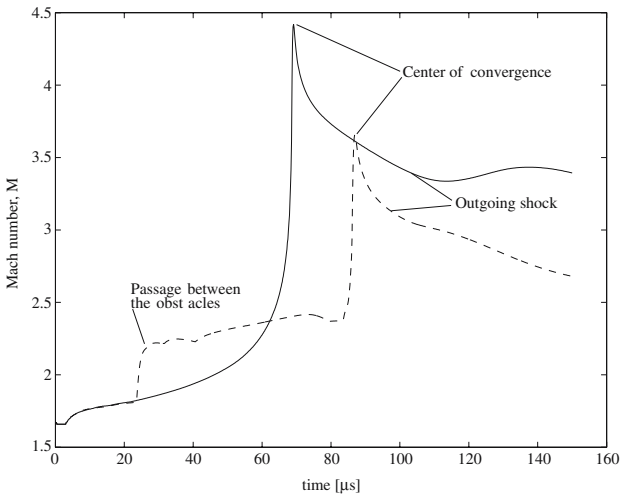

Fig. 23 Comparison of the maximum Mach number in the computational domain for a shock produced by an octagonal boundary, *solid line*, Versus eight cylindrical disturbances, *dashed line*

Acknowledgments This research was initiated in collaboration with Prof. Martin Lesser and his ideas and suggestions are gratefully acknowledged. The authors would like to thank Mr Ulf Landén at KTH Mechanics for careful construction of the cylindrical obstacles. We also would like to thank Dipl. Ing. Ramis Örlü for helping with the cold wire temperature measurements. This work has been financially supported by The Swedish Research Council (VR). This is gratefully acknowledged. The funding from the Göran Gustafsson Foundation provided means for the construction of the shock tube and for acquisition of the experimental equipment which is gratefully acknowledged. We also wish to

express our thanks to Prof. Takayama for his perusal of the manuscript and for the valuable suggestions.

References

1. Apazidis, N., Lesser, M., Tillmark, N., Johansson, B.: An experimental and theoretical study of converging polygonal shock waves. Shock Waves **12**, 39–58 (2002)
2. Apazidis, N., Lesser, M.: On generation and convergence of polygonal-shaped shock waves. J. Fluid Mech. **309**, 301–319 (1996)
3. Watanabe, M., Onodera, O., Takayama, K.: Shock wave focusing in a vertical annular shock tube. In: Brun, R., Dimitrescu, L.Z. (eds.) Shock Waves@Marseille vol. 4, pp. 99–104. Springer, Berlin (1995)
4. Bryson, A.E., Gross, R.W.F.: Diffraction of strong shocks by cones, cylinders, and spheres. J. Fluid Mech. **10**, 1–16 (1961)
5. Eliasson, V., Apazidis, N., Tillmark, N., Lesser, M.B.: Focusing of strong shocks in an annular shock tube. Shock Waves **15**, 205–217 (2006)
6. Perry, R.W., Kantrowitz, A.: The production and stability of converging shock waves. J. Appl. Phys. **22**, 878–886 (1951)
7. Schwendeman, D., Whitham, G.: On converging shock waves. Proc. R. Soc. Lond. A **A413**, 297–311 (1987)
8. Sun, M., Takayama, K.: An artificially upstream flux vector splitting scheme for the euler equations. J. Comput. Phys. **189**, 305–329 (2003)
9. Takayama, K., Onodera, O., Hoshizawa, Y.: Experiments on the stability of converging cylindrical shock waves. Theor. Appl. Mech. **32**, 305–329 (1984)
10. Takayama, K., Kleine, H., Gröning, H.: An experimental investigation of the stability of converging cylindrical shock waves in air. Exp. Fluids **5**, 315–322 (1987)
11. Watanabe, M., Takayama, K.: Stability of converging cylindrical shock waves. Shock Waves **5**, 149–160 (1991)
12. Whitham, G.: A new apporach to problems of shock dynamics. Part 1. Two-dimensional problems. J. Fluid Mech. **2**, 145–171 (1957)
13. Whitham, G.: On the propagation of shock waves through regions of non-uniform area or flow. J. Fluid Mech. **4**, 337–360 (1958)
14. Whitham, G.: A new approach to problems of shock dynamics. Part 2. Three-dimensional problems. J. Fluid Mech. **5**, 369–386 (1959)